Frustrated spin-$\frac{1}{2}$ molecular magnetism in the mixed-valence antiferromagnets $Ba_3MRu_2O_9$ (M = In, Y, Lu)

D. Ziat,[1] A. A. Aczel,[2,*] R. Sinclair,[3] Q. Chen,[3] H. D. Zhou,[3] T. J. Williams,[2] M. B. Stone,[2] A. Verrier,[1] and J. A. Quilliam[1,†]

[1]*Institut Quantique and Département de Physique, Université de Sherbrooke, 2500 Boulevard de l'Université, Sherbrooke, Québec J1K 2R1, Canada*

[2]*Quantum Condensed Matter Division, Oak Ridge National Laboratory, Oak Ridge, Tennessee 37831, USA*

[3]*Department of Physics and Astronomy, University of Tennessee, Knoxville, Tennessee 37996-1200, USA*

(Received 1 February 2017; published 22 May 2017)

We have performed magnetic susceptibility, heat capacity, muon spin relaxation, and neutron-scattering measurements on three members of the family $Ba_3MRu_2O_9$, where M = In, Y, and Lu. These systems consist of mixed-valence Ru dimers on a triangular lattice with antiferromagnetic interdimer exchange. Although previous work has argued that charge order within the dimers or intradimer double exchange plays an important role in determining the magnetic properties, our results suggest that the dimers are better described as molecular units due to significant orbital hybridization, resulting in one spin-1/2 moment distributed equally over the two Ru sites. These molecular building blocks form a frustrated, quasi-two-dimensional triangular lattice. Our zero- and longitudinal-field μSR results indicate that the molecular moments develop a collective, static magnetic ground state, with oscillations of the zero-field muon spin polarization indicative of long-range magnetic order in the Lu sample. The static magnetism is much more disordered in the Y and In samples, but they do not appear to be conventional spin glasses.

DOI: 10.1103/PhysRevB.95.184424

I. INTRODUCTION

The 6H-perovskites, with formula $Ba_3MA_2O_9$, have provided fertile ground for recent discoveries in frustrated quantum magnetism. Materials in this family with magnetic M sites have been shown to exhibit quantum spin-liquid behavior, in particular 6HB-$Ba_3NiSb_2O_9$ [1–3] and $Ba_3IrTi_2O_9$ [4], while others, $Ba_3CuSb_2O_9$ [5–7] and $Ba_3ZnIr_2O_9$ [8], exhibit possible quantum spin-orbital liquids. Furthermore, $Ba_3CoSb_2O_9$ has allowed for some of the first studies on the magnetization process of a truly triangular spin-1/2 antiferromagnet [9–13]. The flexibility of this crystal structure means that we are also at liberty to include magnetic $4d/5d$ transition-metal A-site ions and thereby study spin dimers distributed on a triangular lattice with significant spin-orbit coupling and orbital hybridization. In the case of the ruthenates $Ba_3MRu_2O_9$, where M^{3+} is nonmagnetic, one obtains a triangular lattice of magnetic, mixed-valence Ru dimers. A total of seven electrons occupy each dimer and this leads to the possibility of charge, orbital, and spin degrees of freedom.

For analogous $3d$ transition-metal-based dimer systems with more than two electrons per dimer, Hund's coupling is usually dominant and therefore needs to be treated before turning to intersite effects such as electron hopping and the interdimer Coulomb interaction. However, recent theoretical [14,15] and experimental [16] work has shown that this approach can break down in some $4d$ and $5d$ transition-metal-based dimer systems, where Hund's coupling is expected to be significantly weaker due to the spatially extended d orbitals. This more complicated regime may be realized in the $Ba_3MRu_2O_9$ family, as any simple picture based on dominant Hund's coupling cannot describe all of the known magnetic properties of the Ru dimers.

More specifically, two different magnetic ground states for the Ru dimers in $Ba_3MRu_2O_9$ have been proposed previously that are consistent with dominant Hund's coupling. Doi *et al.* [17] first assumed that all seven electrons were localized at particular Ru sites, which leads to $Ru^{4+/5+}$ charge order within the dimers and antiferromagnetic intradimer exchange. They argued that the latter should produce dimers with a magnetic ground state of total spin $S = 1/2$, which could explain the loss of effective magnetic moment with decreasing temperature in their M = In, Y, and Lu magnetic susceptibility measurements and an entropy release less than $R\ln(2)$ in their specific-heat data at the low-temperature magnetic phase transitions (T_m = 4.5, 4.5, and 9.5 K for In, Y, and Lu).

However, their model fails to explain the very different, monotonic susceptibility in the M = La sample, as the intradimer exchange interaction would have to change dramatically, from strongly antiferromagnetic to strongly ferromagnetic, with only a tiny modification of the crystal structure. Even if that were possible, the model would imply $S = 5/2$ dimers in the La compound, which would lead to much larger values of susceptibility than are measured. Furthermore, subsequent neutron-diffraction measurements of the Y system found no evidence for the required charge ordering within the dimers down to 2 K [18]. For these reasons, the magnetic ground state of the Ru dimers has also been discussed more recently in the context of molecular double exchange [18], but this simple model cannot explain the nonmonotonic T dependence of the magnetic susceptibility, the low-T entropy release in the specific-heat data, and the small ordered moment sizes for the Y and La systems found in neutron diffraction.

This means that there is currently no comprehensive understanding of the magnetic ground states for single Ru dimers in the $Ba_3MRu_2O_9$ family. The collective magnetic

*aczelaa@ornl.gov
†jeffrey.quilliam@usherbrooke.ca

ground states of these materials may also be interesting in their own right, as the interdimer interactions are likely frustrated due to the triangular lattice geometry of the dimers. For these reasons, we have used magnetic susceptibility, heat capacity, muon spin relaxation (μSR), and neutron scattering to investigate both the single dimer and collective magnetic properties of the $M =$ In, Y, and Lu systems.

II. EXPERIMENTAL DETAILS

The polycrystalline samples of $Ba_3MRu_2O_9$ (M = In, Y, and Lu) studied here were prepared by the standard solid-state reaction method. Appropriate amounts of $BaCO_3$, In_2O_3/Y_2O_3/Lu_2O_3 (Y_2O_3 and Lu_2O_3 were predried at 980 °C overnight), and RuO_2 were mixed in agate mortars, compressed into pellets, and annealed for 20 hours in air at temperatures of 900, 1200, and 1300 °C, respectively. Magnetic susceptibility and specific-heat measurements were performed using Quantum Design MPMS and PPMS systems. The dc magnetic susceptibility was measured with a magnetic field of 1 kG. AC susceptibility measurements were also performed at various frequencies (from 333 to 9999 Hz) to look for evidence of spin freezing.

Neutron powder diffraction (NPD) was performed with polycrystalline $Ba_3MRu_2O_9$ (M = In, Y, and Lu) using the HB-2A powder diffractometer of the High Flux Isotope Reactor (HFIR) at Oak Ridge National Laboratory (ORNL). The Lu sample was loaded in a vanadium can and the data were collected at $T = 1.5$ K with a neutron wavelength of 1.54 Å and a collimation of 12′-open-12′. The In and Y samples were loaded in aluminum cans and the data were collected at $T = 3.5$ K with a neutron wavelength of 1.54 Å and a collimation of 12′-21′-6′.

Complementary elastic neutron-scattering measurements were performed on the fixed-incident-energy triple-axis spectrometer HB-1A of HFIR at ORNL, using the same polycrystalline samples. A series of two pyrolytic graphite (PG) crystal monochromators provided the fixed incident energy E_i of 14.6 meV and two highly oriented PG filters were placed in the incident beam to remove higher-order wavelength contamination. A PG analyzer crystal was located before the single He-3 detector for energy discrimination. A collimation of 40′-40′-40′-80′ resulted in an energy resolution at the elastic line of ≈1 meV. The elastic scattering was measured at 1.5 K for all three samples, with higher-temperature background data collected at 20 K for the Lu system and 10 K for the In and Y systems.

Inelastic neutron-scattering (INS) measurements were collected on the direct-geometry time-of-flight chopper spectrometer SEQUOIA of the Spallation Neutron Source (SNS) at ORNL, using the same polycrystalline samples loaded in aluminum cans. Spectra were collected at a variety of temperatures by operating in high-flux mode (elastic resolution of ∼4% E_i) with $E_i = 50$ and 100 meV. The monochromatic incident beam was obtained by using a Fermi chopper rotating at a frequency of either 180 or 240 Hz for $E_i = 50$ and 100 meV, respectively. The background from the prompt pulse was removed with a T_0 chopper operating at 90 Hz. An empty aluminum can was measured in identical experimental conditions for a similar counting time. The resulting spectra were subtracted from the corresponding sample spectra after normalization with a vanadium standard to account for variations of the detector response and the solid angle coverage. This procedure ensured that temperature-independent scattering was removed from the spectra before applying the appropriate Bose corrections to calculate $f(Q)^2\chi''(Q,\omega)$, where $\chi''(Q,\omega)$ is the imaginary part of the dynamic magnetic susceptibility and $f(Q)$ is the magnetic form factor.

Muon spin relaxation measurements were performed at TRIUMF, Canada on the M20 beam line with the LAMPF spectrometer and a He-flow cryostat. Samples were encapsulated in Ag-coated mylar adhesive and suspended between copper supports in the path of the muon beam, where they were cooled by helium vapor to as low as ∼2 K. This style of sample mount and a veto counter behind the sample allow us to almost completely eliminate any background asymmetry. Measurements were taken in zero-field (ZF), longitudinal-field (LF), and weak transverse-field (TF) geometries using forward and backward positron counters to determine the asymmetry, $a(t) = (n_B - \alpha n_F)/(n_B + \alpha n_F)$. α is determined with weak transverse-field measurements in the paramagnetic phase and $a(t)$ is divided by the initial asymmetry to obtain the muon polarization, $P(t)$.

III. SEARCH FOR STATIC CHARGE ORDER

It is important to understand the magnetic ground state of a single Ru dimer before moving on to a discussion of these materials' collective magnetic properties. As shown in Fig. 1(a), each Ru site is in an octahedral oxygen environment, and the Ru dimers form via face-sharing octahedra. It is well known that all three materials crystallize in the space group $P6_3/mmc$ at room temperature, which ensures that both Ru sites forming a dimer are crystallographically equivalent due to the crystal symmetry. However, static charge order is a distinct possibility for these materials upon cooling due to the mixed $Ru^{4+/5+}$ nominal valence, which has been found in isostructural systems with a mixed $Ru^{5+/6+}$ nominal valence such as $Ba_3NaRu_2O_9$ [16]. Neutron powder diffraction (NPD) is a sensitive probe to look for this effect, as one can investigate the T dependence of the charge distribution in the dimers indirectly via Ru-O bond lengths.

Figure 2 shows NPD data collected using $\lambda = 1.54$ Å for $Ba_3MRu_2O_9$, with $T = 1.5$ K for the Lu system and $T = 3.5$ K for the In and Y analogs. Rietveld refinements were performed using FULLPROF [19]. In all cases, we find that the data are best

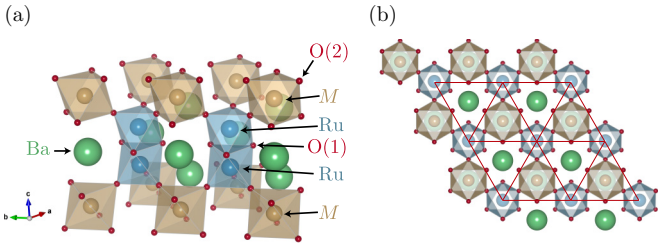

FIG. 1. A portion of the crystal structure of $Ba_3MRu_2O_9$, specifically using parameters for the $M =$ Y sample, showing one plane of Ru-Ru dimers. (a) A view perpendicular to the c axis showing the stacking of Ru ions to form dimers. (b) A view parallel to the c axis, showing the triangular arrangement of Ru dimers.

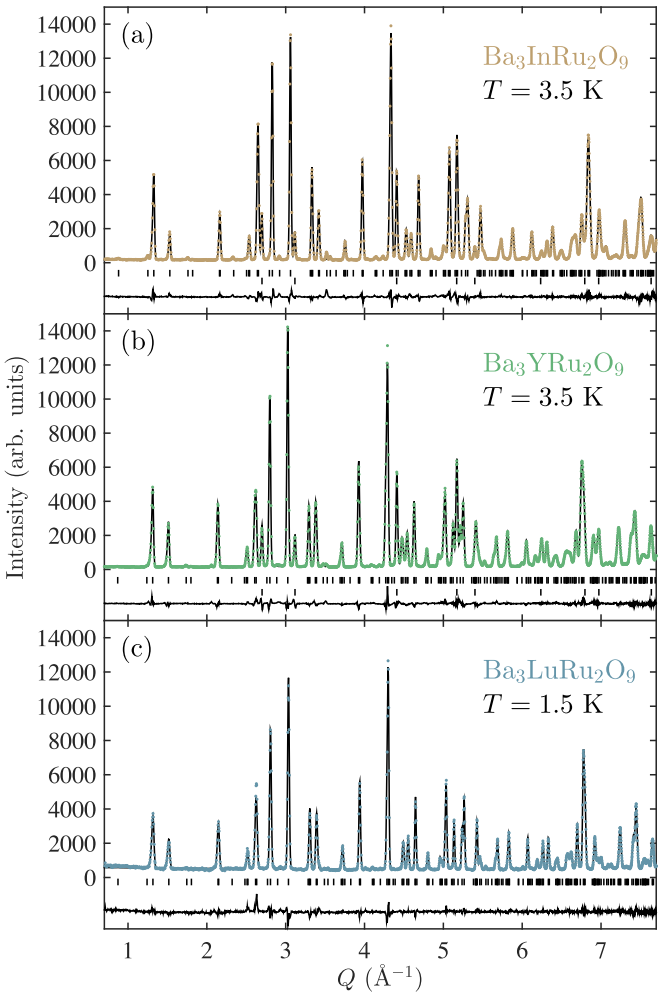

FIG. 2. Neutron powder diffraction measurements with a wavelength of 1.54 Å for (a) $Ba_3InRu_2O_9$ (3.5 K), (b) $Ba_3YRu_2O_9$ (3.5 K), and (c) $Ba_3LuRu_2O_9$ (1.5 K). The corresponding structural refinements (black lines) are superimposed on the data points. The extra peaks in the In and Y patterns arise from the Al sample can.

refined in the room-temperature $P6_3/mmc$ space group with only one unique Ru site and no Ru/M site mixing, and therefore we find no evidence for static charge ordering down to these temperatures. We also do not detect any magnetic Bragg peaks, which would be indicative of long-range magnetic order, in this data. Table I shows lattice constants, atomic fractional coordinates, and selected bond distances and angles extracted from the refinements. We note that our O_2 z parameter for the Y system is significantly different from the value reported in Ref. [18]. Upon careful inspection, their value appears to be somewhat unphysical [20].

IV. MOLECULAR MAGNETISM

Since there is no evidence for static charge order of the Ru dimers in $Ba_3MRu_2O_9$ (M = In, Y, and Lu), we now consider other possibilities for the single dimer ground states that are consistent with the known magnetic properties. We first revisit the dc magnetic susceptibility of these materials, as a satisfactory explanation for the complex T dependence

TABLE I. Structural parameters for $Ba_3MRu_2O_9$ (M = In, Y, and Lu) extracted from the refinements of the $\lambda = 1.54$ Å neutron powder diffraction data. The lattice constants and bond distances are in Å and the bond angles are in degrees. The temperatures at which the measurements were performed are quoted in parentheses on the first line of the table.

B'	In (3.5 K)	Y (3.5 K)	Lu (1.5 K)	La (11 K) [18]
a	5.7947(1)	5.8565(1)	5.8436(1)	5.9492
c	14.2738(2)	14.4589(1)	14.3978(2)	14.9981
Ba_2 z	0.9116(2)	0.9075(1)	0.9084(2)	0.8909
Ru z	0.1611(1)	0.1632(1)	0.1620(1)	0.16556
O_1 x	0.4874(5)	0.4879(4)	0.4887(5)	0.4873
O_2 x	0.1712(4)	0.1758(2)	0.1741(3)	0.17889
O_2 z	0.4150(1)	0.4124(1)	0.4138(1)	0.40471
R_{wp}	8.82%	6.27%	6.18%	6.66%
Ru-O_1	2.001(3)	2.009(2)	2.019(2)	2.030
Ru-O_2	1.956(2)	1.936(1)	1.947(2)	1.909
Ru-Ru	2.538(3)	2.511(2)	2.533(3)	2.533
Ru-O_1-Ru	78.8(1)	77.4(1)	77.7(1)	77.2

is still lacking. Our own results, shown in Fig. 3(c), are very similar to previous work by Doi *et al.* [17]. Between ∼100 and 300 K, χ is an increasing function of temperature ($d\chi/dT > 0$), suggestive of gapped spin excitations. Below ∼100 K, however, χ becomes a decreasing function of temperature ($d\chi/dT < 0$), i.e., begins to resemble a Curie-Weiss law. A logical explanation for this nonmonotonic behavior is a change in spin number with temperature. For example, the ground state

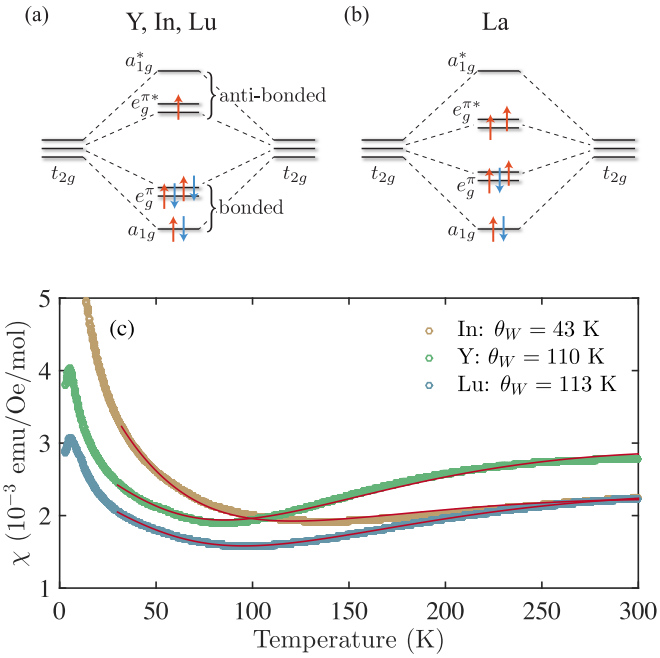

FIG. 3. (a) Energy-level and spin occupation diagram for a hybridized $Ru^{4.5+}$-$Ru^{4.5+}$ dimer with large bonding energy, which is likely to apply to the In, Y, and Lu samples [15]. (b) Energy-level diagram with lower bonding energy as expected to apply to the La sample. (c) Magnetic susceptibility of the In, Y, and Lu samples, with the fits using Eq. (1) superimposed on the data.

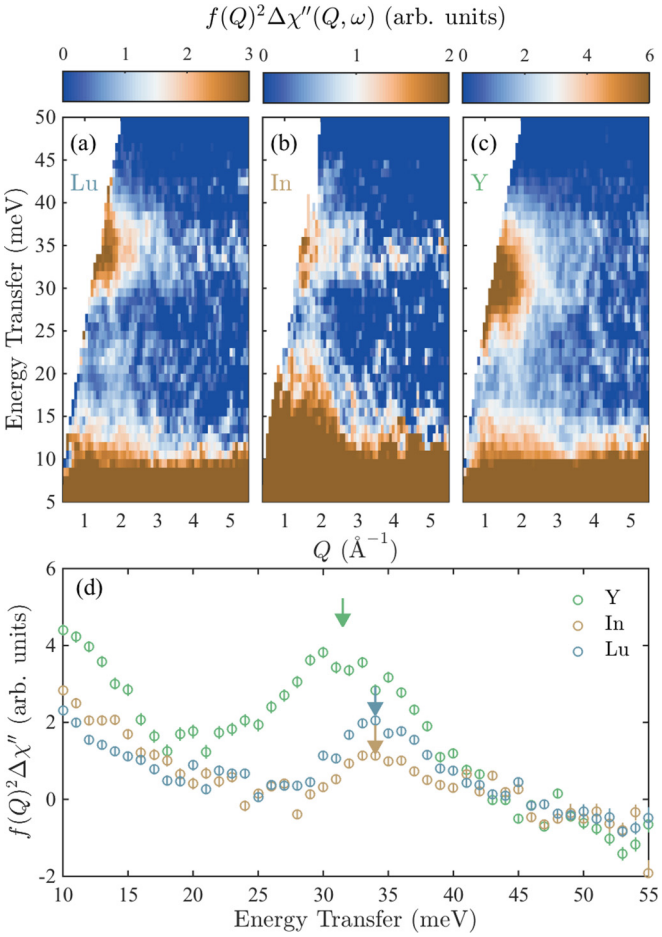

FIG. 4. $f(Q)^2\Delta\chi'' = f(Q)^2\chi''(5\text{ K}) - f(Q)^2\chi''(225\text{ K})$ (arbitrary units) obtained with inelastic neutron scattering for (a) $Ba_3LuRu_2O_9$, (b) $Ba_3InRu_2O_9$, and (c) $Ba_3YRu_2O_9$ as a function of wave vector and energy transfer. (d) Cuts of $f(Q)^2\Delta\chi''$ integrated between $Q = 2$ and 2.5 Å^{-1}.

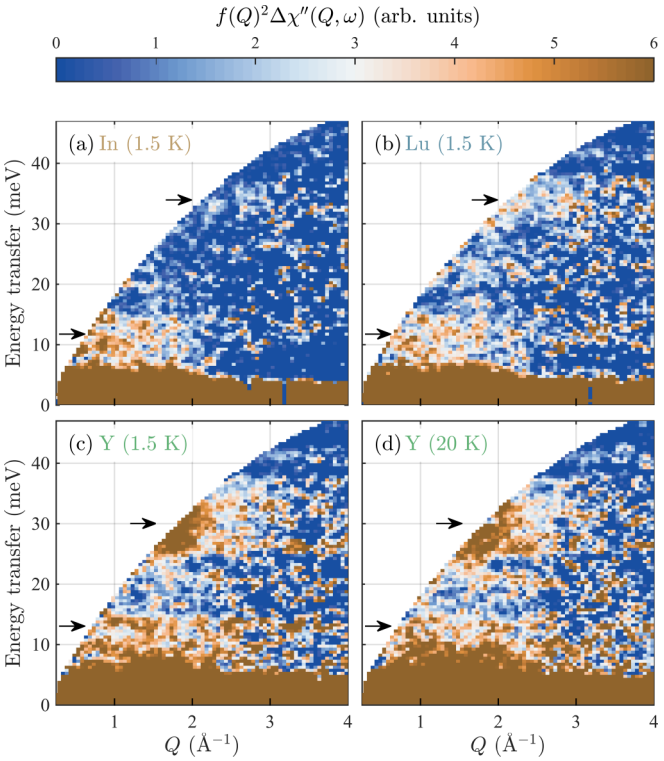

FIG. 5. $f(Q)^2\Delta\chi'' = f(Q)^2\chi''(T) - f(Q)^2\chi''(225\text{ K})$ (arbitrary units) obtained with inelastic neutron scattering as a function of wave vector and energy transfer, using a lower incident energy of $E_i = 50$ meV for (a) $Ba_3LuRu_2O_9$ at $T = 1.5$ K, (b) $Ba_3InRu_2O_9$ at $T = 1.5$ K, and $Ba_3YRu_2O_9$ at (c) $T = 1.5$ K and (d) $T = 20$ K.

of each Ru dimer may be a $S = 1/2$ doublet with a relatively low-lying excited $S = 3/2$ manifold (with energy Δ_1). As $T > 100$ K, we begin to populate the $S = 3/2$ manifold, which naturally has a larger susceptibility. If we assume that there is also a $S = 5/2$ manifold with higher energy Δ_2, a minimal functional form for the susceptibility [17] can be written as

$$\chi(T) = \frac{\mathcal{C}}{T + \Theta_W}\frac{1 + 10e^{-\Delta_1/k_BT} + 35e^{-\Delta_2/k_BT}}{1 + 2e^{-\Delta_1/Tk_B} + 3e^{-\Delta_2/k_BT}}. \quad (1)$$

This equation accounts for interactions between dimers via the Θ_W term. Fits of this form provide an adequate description of the susceptibility data over a broad temperature range. Without fixing any parameters, these fits yield $\Delta_1 = 38.9(4)$ (In), 28.6(3) (Y), and 34.1(4) meV (Lu). However, fits of this form are somewhat overparametrized and a more direct method for exploring the excitation spectrum is desirable.

To this end, we have employed inelastic neutron-scattering measurements, carried out on the SEQUOIA spectrometer with an incident energy of $E_i = 100$ meV. We plot $f(Q)^2\chi''(Q,\omega)$ for $Ba_3MRu_2O_9$ in Figs. 4(a)–4(c) as a temperature difference $f(Q)^2\Delta\chi'' = f(Q)^2[\chi''(5\text{ K}) - \chi''(225\text{ K})]$ to isolate the low-temperature magnetic scattering. Two dispersive magnetic modes are visible in the spectra of each system. The lower modes are located just above the elastic line and appear more clearly in the complementary $E_i = 50$ meV datasets shown in Fig. 5. The finite dispersion of these modes likely arises from significant interdimer interactions. Constant-Q cuts taken from the same datasets with an integration range of 2–2.5 Å^{-1} are depicted in Fig. 4(d). These cuts indicate that the higher-energy mode is centered about 34(1), 31.5(1.5), and 34(1) meV for the In, Y, and Lu systems, respectively. These excitation energies correspond reasonably well to the values of Δ_1 obtained from freely fitting the dc susceptibility.

Ultimately, we have fitted the susceptibility data by fixing the values of Δ_1 to those measured with our INS measurements, resulting in only three-parameter fits and eliminating the overparametrization problem. The Curie constants $\mathcal{C}$ obtained from this fitting give effective moment sizes μ_{eff} in the ground-state manifold of $1.40(3)\mu_B$, $1.65(3)\mu_B$, and $1.53(3)\mu_B$ per dimer for the In, Y, and Lu samples, respectively. These values are only slightly under the value of $1.73\mu_B$ expected for a free spin-1/2, and therefore this result is consistent with our proposal that a single dimer has a total spin $S = 1/2$ ground state. The Weiss constants Θ_W are found to be 43(3), 110(10), and 113(2) K for the In, Y, and Lu systems, respectively, which are indicative of significant antiferromagnetic interdimer exchange. The $S = 5/2$ state is found at $\Delta_2 = 81(1)$ (In), 72(1) (Y), and 80(1) meV (Lu).

Despite the high energy of Δ_2, these states cannot be ignored in the susceptibility fitting.

This model includes a number of simplifications, most importantly that the Weiss constant Θ_W is the same in all manifolds of total spin. This is counterintuitive since one would expect a higher total spin to yield a larger Weiss constant, all things being equal, since $\Theta_W = 2zJS(S+1)/3k_B$, where z is the number of nearest neighbors (NN). The success of this simplistic model, in which Θ_W is constant, therefore implies that the interaction strength J between dimers is smaller when they are excited into their $S = 3/2$ or $S = 5/2$ manifolds, compensating for the increase in spin number.

This single dimer picture supported by our susceptibility and INS measurements can be better understood by drawing on the work of Streltsov and Khomskii, who have investigated the possibility of covalent bonds forming between $4d/5d$ ions in various cases [14,15]. For the current $Ba_3MRu_2O_9$ structure, one should consider the transition-metal Ru ions in the strong crystal field regime. Since these ions are in an octahedral oxygen environment, this assumption leads to the usual low-energy t_{2g} orbitals and higher-energy e_g orbitals. A trigonal distortion, inherent to this family of materials crystallizing in the $P6_3/mmc$ space group, then splits the t_{2g} orbitals into an a_{1g} singlet and an e_g^π doublet [21]. The unique face-sharing octahedral geometry of two neighboring Ru sites is argued to produce strong orbital hybridization, with the a_{1g} orbitals experiencing the largest bonding energy, as shown in Figs. 3(a) and 3(b). If the two Ru sites are close enough, then the e_g^π orbitals can also participate in molecular bonding. The choice of magnetic ground state for a single dimer in a particular system depends critically on the ratio of the molecular bonding energy to Hund's coupling, as illustrated in Figs. 3(a) and 3(b). In the present materials, $Ba_3MRu_2O_9$ with M = Y, In, and Lu, the molecular bonding energy appears to be higher than Hund's coupling, and therefore the electrons prefer to occupy the e_g^π bonding orbitals rather than the $e_g^{\pi*}$ antibonding orbitals. In other words, three covalent bonds form and one uncompensated electron is left over. This situation is illustrated in Fig. 3(a).

This model suggests that the higher-energy dispersive modes observed in the INS spectra, shown in Figs. 4(a)–4(c) and highlighted in the cuts of Fig. 4(d), can be assigned to electron transitions from bonding to antibonding molecular orbitals, which would cause the total spin of a dimer to change from $S = 1/2$ to $3/2$. The origin of the lower-energy INS modes can also be understood in the context of the molecular magnet model, as they may simply represent electron transitions between the antibonding orbitals shown in Fig. 3(a). Any origin associated with collective magnetic ordering or spin freezing for these low-energy modes can be ruled out as there was no significant change observed in their temperature dependence between 1.5 and 20 K in complementary $E_i = 50$ meV datasets. This is illustrated for $Ba_3YRu_2O_9$ in Fig. 5.

On the other hand, the magnetic susceptibility of $Ba_3LaRu_2O_9$ [17] is consistent with a total spin $S = 3/2$ dimer ground state and a $S = 1/2$ excited state, which implies that the molecular bonding energy is not as large and therefore only two covalent bonds form in this case, as illustrated in Fig. 3(b). This also explains the much larger magnetic moment observed in neutron-diffraction experiments [18]. It is natural to ask what structural parameter gives rise to this dramatic difference between the La sample and the In, Y, and Lu analogs studied here. Although there is no discernible correlation with Ru-Ru distance, as shown in Table I, the La sample does have a larger Ru-O(1) distance and smaller Ru-O(1)-Ru bond angle than the other materials. These parameters may play an important role in determining the molecular bonding energy of the e_g^π orbitals, especially since the O_1 ions form the common octahedral face of the Ru_2O_9 units. As can be seen from Fig. 3(b), a smaller bonding energy leads to the $S = 3/2$ configuration expected for the La sample.

V. COLLECTIVE MAGNETIC GROUND STATES

Specific heat, presented in Fig. 6(a), shows peaks at T_m = 3.0, 5.2, and 10.5 K for the In, Y, and Lu samples, respectively,

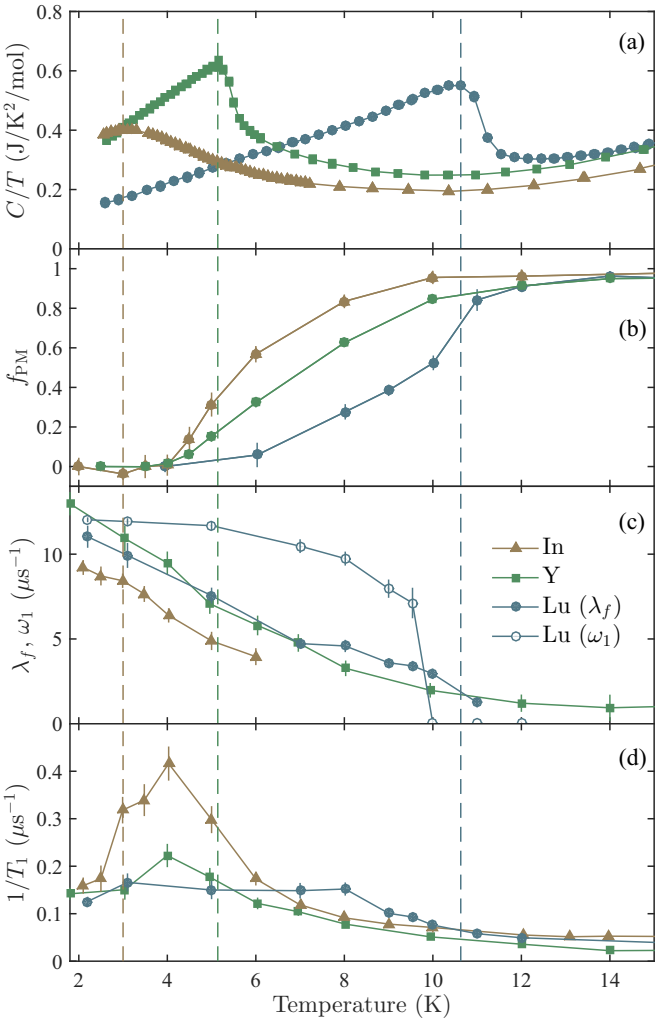

FIG. 6. (a) Specific heat (C) of the samples measured here with dashed lines identifying the low-T anomalies as T_m. (b) The paramagnetic fraction of the samples as a function of temperature, obtained by applying a transverse field and assessing the amplitude of the μ^+ precession generated. (c) Fast-relaxation rates λ_F for all three samples and the highest oscillation frequency in the Lu sample, $\omega_1 = 2\pi f_1$, as functions of temperature. (d) Slow-relaxation rate, or $1/T_1$, vs temperature for all three samples.

presumably indicating the onset of long-range order (LRO) or spin freezing. First, it is quite clear that these materials are highly frustrated as the values of Θ_W we have determined are much higher than T_m, with the frustration likely arising from the triangular lattice geometry of the Ru dimers and the strong antiferromagnetic interactions between them. More specifically, we find frustration parameters $f = \Theta_W/T_m$ of 13 (In), 21 (Y), and 11 (Lu). Note that the suppression of these materials' transition temperatures, relative to their Weiss constants, may just as easily be driven by low dimensionality (that is, weak interactions between the triangular planes) rather than by geometric frustration.

While our results are qualitatively consistent with previous work [17], there is some variability in transition temperatures between our samples and those of Doi *et al.* [17]. Whereas our M = Lu sample has a peak in the specific heat $C(T)$ at 10.5 K, their sample seems to have a 9.5 K ordering transition. The low-T specific-heat anomaly of our M = Y sample is also somewhat elevated when compared to Doi *et al.* [17]. Meanwhile, our M = In sample has a peak in $C(T)$ that is broader and somewhat lower in temperature. Evidently there is some sample dependence of the magnetic properties of these materials.

Since there are possible indications of magnetic order or spin freezing in the $C(T)$ measurements, we performed elastic neutron scattering on the $Ba_3MRu_2O_9$ (M = In, Y, and Lu) samples using the HB-1A fixed-incident-energy triple-axis spectrometer at HFIR of ORNL. The HB-1A experiment was designed to maximize the possibility of observing a magnetic signal, so this data is complementary to the HB-2A measurements described above where magnetic Bragg peaks were not observed. Specific advantages of the HB-1A experiment, as compared to the HB-2A measurements, are as follows. First, the low-T datasets were all measured at $T = 1.5$ K to ensure that we were well below the $C(T)$ anomalies in each case. Second, the signal-to-noise ratio at HB-1A is enhanced, relative to that of HB-2A, due to a double-bounce monochromator and the use of an analyzer for energy discrimination. Despite these improvements in the experimental setup, the HB-1A measurements show no evidence of a magnetic signal below the $C(T)$ anomalies in each case, as illustrated in Fig. 7. Although the HB-1A result for the Y sample appears to be inconsistent with previous work by Senn *et al.* [18] using the WISH diffractometer at ISIS, it is important to note that the magnetic Bragg peaks observed in the WISH experiment were extremely weak. In fact, the ordered moment for the Y system reported in Ref. [18] is only $0.5(6)\mu_B$ per Ru site, so there is a great deal of uncertainty in this value. The apparent discrepancy with the HB-1A data may simply arise due to a slightly different signal-to-noise ratio on WISH as compared to HB-1A, or there may be an extreme sensitivity of the Y magnetic ground state to some form of disorder.

Reference [18] also reported the observation of significantly stronger magnetic Bragg peaks for $Ba_3LaRu_2O_9$. An ordered moment of $1.4(2)\mu_B$ per Ru site was determined from the subsequent magnetic refinement, which is consistent with a total spin of $S = 3/2$ per dimer. Similar magnetic reflections were observed for both the La and Y samples, and this finding led the authors to conclude that these two materials host the same magnetic structure. Specifically, they find a (0 1/2 0) propagation vector, which they attribute to a magnetic structure with ferromagnetic dimers. We note that their assumption of a ferromagnetic intradimer interaction is not consistent with our interpretation of the single dimer ground state for these materials, as discussed above. However, this discrepancy is resolved simply by replacing the single ion spins in their work with a single spin-1/2 moment distributed over each dimer in the case of the Y sample or a spin-3/2 moment in the case of La. The revised magnetic structure is then simply a collinear stripe phase, which has been predicted to arise for the quasi-two-dimensional triangular lattice when the NN and next-nearest-neighbor (NNN) in-plane exchange interactions are antiferromagnetic and comparable in magnitude [22]. These materials could therefore be considered to be the molecular magnet equivalents of isostructural compounds (for instance, $Ba_3CoSb_2O_9$ [9–13]) where the M site is magnetic and forms a quasi-two-dimensional triangular lattice, albeit with a more important NNN interaction strength.

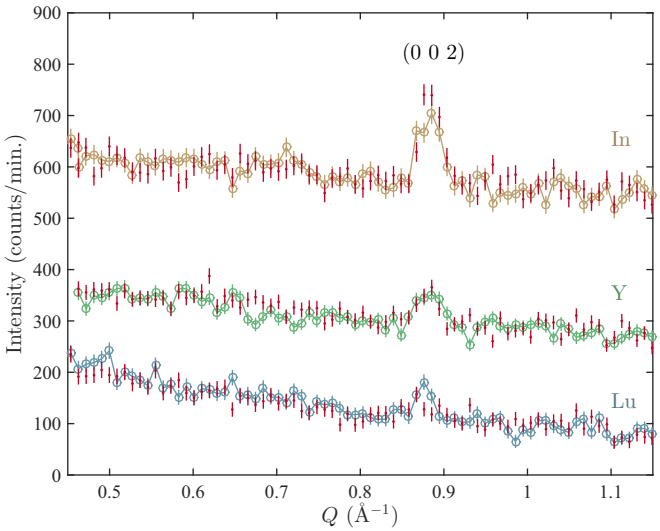

FIG. 7. Elastic neutron-diffraction data from HB-1A for all three samples. The open circles are data taken at 1.5 K. Red points were taken above T_m, at 10 K (for Y and In) and 20 K (for Lu). The Lu data have been shifted downwards by 200 counts/minute for ease of view. No evidence of magnetic order is observed, possibly because the ordered moment is extremely small or spread out over an entire dimer.

Since our neutron-scattering measurements found no evidence for magnetic Bragg peaks in the In, Y, and Lu samples, possibly due to the small ordered moment sizes, it is natural to study these materials with μSR, which is one of the most sensitive probes of weak magnetism. As can be seen in Fig. 8, the ZF-μSR data of all three samples show indications of a magnetic phase transition with greatly increased relaxation at low T. The In and Y samples do not show any oscillations of the muon spin polarization, and thus the fast relaxation may arise from static disordered magnetism or slow spin fluctuations. As shown in Figs. 8(a) and 8(b), the muon spin polarization is well described by the following two-component relaxation function:

$$P(t) = (1-x)e^{-\lambda_f t} + xe^{-t/T_1}, \qquad (2)$$

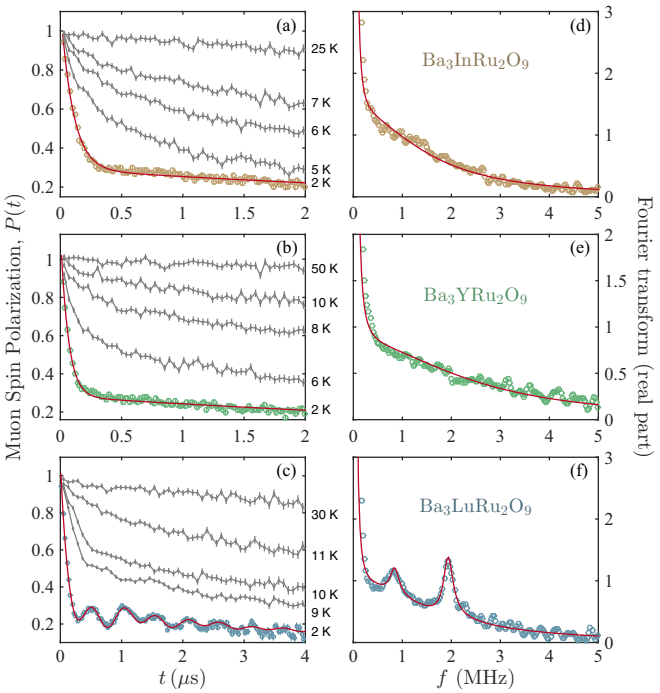

FIG. 8. Zero-field μSR asymmetry at various temperatures for (a) In, (b) Y, and (c) Lu, with the corresponding fits superimposed on the 2 K data only. Fourier transforms of the 2 K data, with the fits superimposed, are shown in (d) In, (e) Y, and (f) Lu. The Lu sample data show long-lived oscillations, whereas the data of the In and Y samples show only fast exponential relaxation (along with a slowly relaxing 1/3 tail). The narrow zero-frequency peak in the Fourier transforms comes from the T_1 time of the 1/3 tail, and is a measure of spin fluctuations rather than static internal fields.

where x is close to 1/3 at low T and $1/T_1$ is the spin-lattice relaxation rate [23]. Assuming that we are in the quasistatic limit, λ_f results largely from inhomogeneities (disorder) in the static internal fields at the muon site(s), whereas $1/T_1$ is caused by residual spin fluctuations.

As shown in Fig. 8(c), clear oscillations of the polarization are observed in the low-T regime for the Lu sample. The Fourier transform of this data, illustrated in Fig. 8(f), shows two distinct frequencies corresponding to rather small internal fields of 6.1(2) and 14.1(1) mT. The two frequencies are indicative of two distinct muon stopping sites, which can likely be associated with the two crystallographically inequivalent oxygen atoms in the crystal structure. It is also possible that one crystallographic muon stopping site could give rise to two distinct frequencies as a result of a complex magnetic structure. However, the magnetic structure reported by Senn *et al.* [18] should only lead to one frequency per crystallographic site, so in that particular case our spectrum would arise from two crystallographically distinct muon stopping sites.

The Fourier transform also shows that these two peaks are superimposed on a broad feature, which is consistent with the fast exponential relaxation observed in the time domain. Hence, the Lu data can be fit with the following equation:

$$P(t) = (1-x)\sum_{n=0}^{2} a_n \cos(2\pi f_n t)e^{-\lambda_n t} + xe^{-t/T_1}, \quad (3)$$

TABLE II. Various experimental parameters for the three samples studied. The transition temperature T_m is obtained from the maximum in specific heat. The first energy gap to the $S = 3/2$ excited state, Δ_1, is obtained from inelastic neutron scattering. The magnetic susceptibility allows for a determination of the Weiss constant Θ_W, the effective moment μ_{eff}, and the second energy gap to the $S = 5/2$ excited state, Δ_2. From μSR, the muon oscillation frequencies f_1 and f_2, the corresponding line widths λ_1 and λ_2, and the fast-relaxation rate λ_f are presented.

Technique	Parameter	In	Y	Lu
C	T_m (K)	3.0(3)	5.2(1)	10.5(2)
INS	Δ_1 (meV)	34.0(1.0)	31.5(1.5)	34.0(1.0)
χ	Δ_2 (meV)	81(1)	72(1)	80(1)
	Θ_W (K)	43(3)	110(10)	113(2)
	μ_{eff}/μ_B	1.40(3)	1.65(3)	1.53(3)
μSR	λ_f (μs^{-1})	9.9(3)	15.7(6)	10.9(7)
	f_1 (MHz)			0.83(3)
	λ_1 (μs^{-1})			0.7(4)
	f_2 (MHz)			1.91(2)
	λ_2 (μs^{-1})			0.74(16)

where $f_0 = 0$ and $\lambda_0 = \lambda_f = 10.9(7)$ μs^{-1} is the fast-relaxing exponential component. Despite the fact that the oscillations in the muon spin polarization are very well resolved, our fits reveal that they come from a relatively small portion of the sample, 15%, with the remainder of the sample behaving more similarly to the In and Y analogs. The fitting parameters obtained in ZF at the lowest temperatures are presented in Table II.

TF-μSR measurements (in a field of ∼50 G) were used to rapidly map out the transitions. The data was fit with the following equation:

$$P(t) = f_{\text{PM}} \cos(\gamma B_{\text{TF}} t + \phi)e^{-\lambda t} + (1 - f_{\text{PM}}), \quad (4)$$

where f_{PM}, shown as a function of temperature in Fig. 6(b), is the fraction of the sample that remains paramagnetic (and therefore has oscillations of the muon spin polarization induced by the applied magnetic field). The other fraction of the sample hosts either static magnetism or strong spin dynamics that dwarf the small applied transverse field. It is interesting to compare the temperature evolution of the paramagnetic fraction to the specific heat, the maximum of which can be taken as the transition temperature T_m. For the Lu sample, f_{PM} begins to drop below 100% precisely at T_m. On the other hand, the paramagnetic volume fraction deviates from 100% well above T_m for the In and Y samples, which suggests that there is a broad temperature regime of short-range magnetic order.

Performing ZF-μSR measurements as a function of T has allowed us to extract the temperature dependence of $1/T_1$ as well as the fast-relaxation rate λ_f. In the case of the Lu system, we can also track one of the precession frequencies, f_1, as a function of temperature, whereas the lower frequency f_2 is only quantifiable at the lowest temperatures. These results are shown in Figs. 6(c) and 6(d). $f_1(T)$ develops rather sharply at the Lu transition temperature and the T dependence resembles a standard order-parameter plot. On the other hand, λ_f evolves

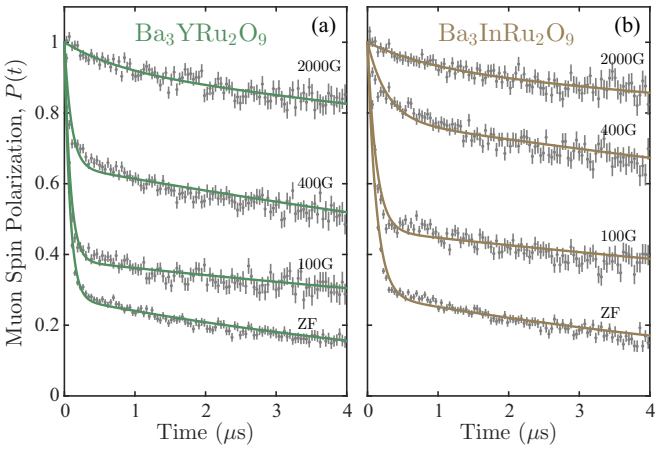

FIG. 9. Longitudinal-field μSR scans for the Y and In samples.

very gradually for all three samples with no sharp change at T_m. $1/T_1$ shows a peak near 4 K in the data for the Y and In samples, which is typical of critical spin dynamics. In the case of the Lu sample, there is a much weaker and broader feature in $1/T_1$.

The two-component exponential relaxation observed in the Y and In samples could be interpreted in two ways. First, in a quasistatic picture, the slow relaxation arises from a so-called 1/3 tail with a weak $1/T_1$ relaxation rate coming from residual spin fluctuations, and the fast relaxation is the 2/3 component coming from random internal fields. Alternatively, one could suspect a dynamic, but inhomogeneous material with two different T_1 times. Longitudinal-field scans at the lowest temperature, shown in Fig. 9, confirm that the fast relaxation is a result of static inhomogeneities as it is decoupled fairly quickly. More precisely, in the Y sample, the fast relaxation is $\lambda_f = 15.7(6)\ \mu s^{-1}$, implying an internal field distribution of width $\Delta B \simeq \lambda_f/\gamma_\mu = 184(7)$ G. Thus, the application of a longitudinal field equal to $B_{\rm LF} = 10\Delta B$ should entirely decouple the muon spins from the internal field and eliminate the fast-relaxing 2/3 component of $P(t)$ [24]. As shown in Fig. 9(a), this appears to be the case for the LF = 2000 G spectrum. Furthermore, as seen in Fig. 9(b), the ZF fast relaxation for the In sample [$\lambda_f = 9.9(3)\ \mu s^{-1}$] is somewhat more easily decoupled via application of a longitudinal field, as expected. It is thus clear that these materials host static magnetic ground states from the perspective of μSR.

It is tempting to attribute the lack of oscillations in the ZF muon spin polarization of the In and Y samples to spin-glass physics, especially since a zero-field-cooled/field-cooled divergence has been previously observed at T_m in the dc susceptibility of the former system [25]. Furthermore, many geometrically frustrated magnetic materials show a strong sensitivity to tiny amounts of quenched crystalline disorder which can lead to a spin-glass transition [26–29]. However, we have also measured the ac susceptibility of these materials at several different frequencies (ranging from 333 to 9999 Hz) and found no evidence of spin glassiness. More specifically, as shown in Fig. 10, the position $T_{\rm max}$ of the real part of the ac susceptibility, $\chi'(T)$, is independent of frequency in the frequency range studied. A conventional spin glass will show a maximum in χ' at the freezing temperature T_f, which then

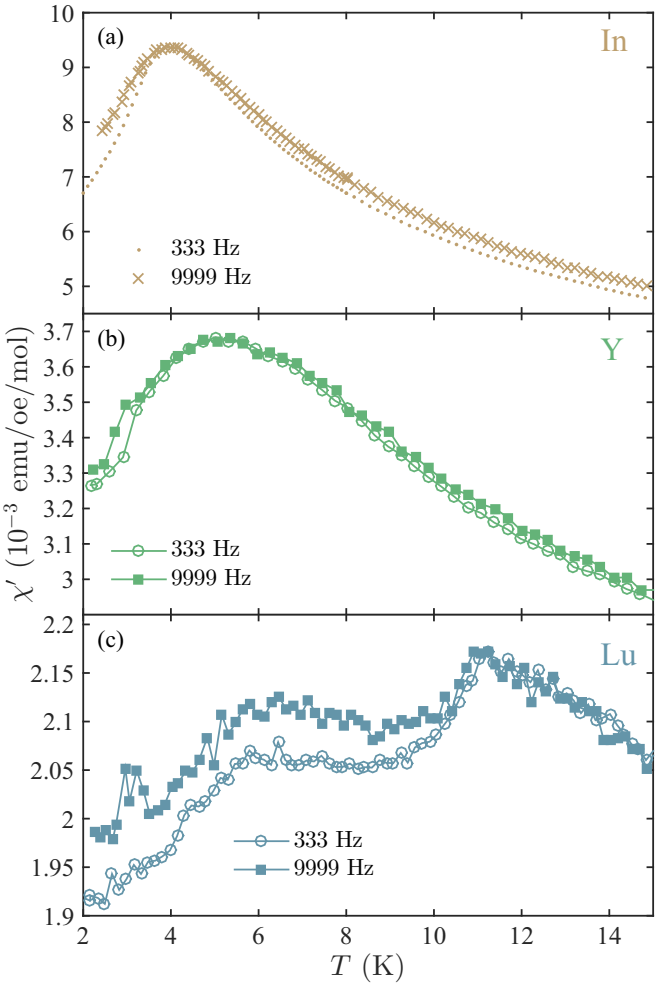

FIG. 10. AC susceptibility (χ') of all three samples at two different frequencies, 333 and 9999 Hz. The high-frequency data has been normalized so that the peak susceptibilities are equal, since the frequency response of the PPMS system is not perfectly flat. Otherwise, the temperature dependence of the susceptibilities is very similar. In particular, the peak positions are independent of frequency.

depends strongly on the frequency of measurement, with an extrapolation to zero frequency allowing for a determination of the true glass temperature T_g [30]. Whereas the In and Y samples have a single peak in χ', the Lu sample has a somewhat more complicated susceptibility, with a relatively sharp peak at ~11 K, corresponding to the peak in specific heat and the onset of oscillations in μSR and a lower-temperature peak, similar to that of the Y sample, which likely corresponds to the gradual onset of fast relaxation (λ_f) in the μSR spectra. In other words, the broad, lower-temperature peak is associated with the disordered portion of the sample. Nonetheless, this peak does not seem to show an appreciable dependence on frequency, but simply a very slight increase in magnitude at 9999 Hz. These two features end up forming a rather broad critical-temperature regime which is consistent with the broad $1/T_1$ feature observed in our μSR experiments on the Lu sample. Given our ac susceptibility results and the fact that magnetic Bragg peaks were observed in neutron-diffraction measurements on a different Y sample [18], it appears that

these materials are not conventional spin glasses and likely have long-range ordered ground states.

There are several possible origins for strongly damped oscillations in the μSR data. We will concentrate on static origins only, since the well-defined 1/3 tail in our data indicates that the spins are mostly static, or fluctuating so slowly that they are essentially static from the point of view of μSR. The two possible static origins of the strong damping are (1) a large number of inequivalent muon stopping sites and (2) a modulation of the internal fields by disorder. The first scenario is highly unlikely given the two well-defined oscillations in the Lu data, which imply that there are two preferred crystallographic sites for the muons. On the other hand, the second scenario appears to be compatible with our μSR and neutron-scattering results. An antiferromagnetic, symmetry-breaking long-range order can coexist with a large random modulation of the moments. This large amount of disorder can lead to the loss of oscillations in the ZF muon spin polarization and a reduced magnetic signal in neutron scattering that is not observed in our measurements. Given the discrepancy between our results and earlier neutron-diffraction work on the Y system [18], it is logical to suspect the influence of sample-dependent disorder on the magnetic ground state.

It is also valuable to consider the implications of the observed μSR signals for the molecular magnet model proposed above, notably through the size of the measured internal fields. Dipolar coupling to pointlike dipoles of $0.5\mu_B$ per site ($S = 1/2$ per dimer) should give rise to an oscillation frequency of $\sim$7 MHz for a μ^+ stopping $\sim$1 Å away from the O_1 site. Hence, the fact that we observe $f_1 = 1.91(2)$ MHz in the Lu sample implies a magnetic moment of only $0.14\mu_B$ ($0.28\mu_B$ per dimer). Evidently a model of pointlike dipoles on the Ru sites is highly simplistic. Even so, our results indicate that the spins are probably very much extended over an entire Ru_2O_9 "molecule," which is consistent with the orbital hybridization picture discussed above. Indeed, the slow oscillations seen here resemble those observed in molecular magnets where each spin is distributed over an entire molecular unit [31,32]. The ordered magnetic moments for the Y and In samples appear to be similarly weak, which is likely why no magnetic signal was detected in our elastic neutron-diffraction measurements.

Finally, we can speculate as to why the Y and In samples show such a high level of disordered static magnetism. As can be seen in Figs. 3(a) and 3(b), the e_g^π and $e_g^{\pi *}$ orbitals remain degenerate in the $Ba_3MRu_2O_9$ structure. For the Lu, Y, and In samples, only one electron occupies the antibonding $e_g^{\pi *}$ orbitals and therefore they are Jahn-Teller (JT) active. Importantly, this degeneracy is not lifted by the spin-orbit coupling [21]. This may leave these materials vulnerable to local structural distortions that relieve the degeneracy, but lead to disorder in the interdimer exchange or the crystalline electric field, both of which can modulate the size of the ordered moments. An important parallel can be found in the sister compound $Ba_3CuSb_2O_9$, which is also based on $S = 1/2$ moments and Jahn-Teller active [6]. In $Ba_3CuSb_2O_9$, two distinct behaviors are observed, depending on the precise stoichiometry of the samples [6,33]. In some off-stoichiometric samples, the orbital degeneracy is relieved by an orthorhombic distortion (a collective JT transition) near 200 K. Ultimately, these orthorhombic samples order magnetically at low temperatures. More stoichiometric samples manage to preserve their room-temperature hexagonal symmetry down to much lower temperatures, either through a dynamic JT effect [34] or else local distortions that nonetheless preserve the global symmetry of the structure and give rise to a random-singlet magnetic ground state [7]. The most recent experimental results, i.e., thermal-conductivity measurements, on nearly stoichiometric single-crystal $Ba_3CuSb_2O_9$, point toward the local-distortion picture [35], which is consistent with the random singlet magnetic ground state and excitation gap [7]. Since a hexagonal to orthorhombic collective JT transition can be ruled out by the neutron-diffraction results on the materials studied here, similar random distortions might then apply, and they may be extremely important for understanding the collective magnetic ground states and possible sample dependence of the magnetic properties. Future work should search for these local distortions, possibly via x-ray absorption fine-structure measurements.

VI. CONCLUSIONS

We have used a wide array of experimental techniques to characterize both the single dimer and collective magnetic properties of the mixed-valence Ru dimer systems $Ba_3MRu_2O_9$ (M = In, Y, and Lu). Our combined neutron powder diffraction, dc magnetic susceptibility, and inelastic neutron-scattering results indicate that the Ru dimers are best described as molecular units with one spin-1/2 moment distributed equally over the two Ru sites. Two dispersive magnetic excitations are observed in the inelastic neutron-scattering spectrum of each system. We attribute the lower-energy mode to electron transitions between antibonding orbitals, while the upper mode is argued to arise from electron transitions between bonding and antibonding orbitals.

The dimers form a quasi-two-dimensional triangular lattice, which is strongly frustrated due to significant antiferromagnetic interdimer exchange. Our heat capacity and muon spin relaxation results reveal that the molecular moments develop a static magnetic ground state in each case, with clear evidence of long-range magnetic order for the Lu sample. The size of the static internal fields observed in μSR at low temperatures is consistent with $S = 1/2$ moments distributed over an entire Ru_2O_9 dimer, similar to molecular magnets. Although the static magnetism is much more disordered for the Y and In samples, they do not appear to be conventional spin glasses. Overall, the current work demonstrates that the 6H-perovskites $Ba_3MA_2O_9$ are excellent model systems for detailed investigations of frustrated quantum magnetism arising from spin-1/2 molecular building blocks on a triangular lattice. Given the strong theoretical interest in $S = 1/2$ triangular-lattice antiferromagnets and the rarity of representative materials, these systems should be attractive for future studies of the magnetic ground state and magnetization process, albeit with the added complexity of orbital degrees of freedom. Finally, we note that our results can likely be directly applied to understanding the magnetic properties of the related Ir-dimer system, $Ba_3InIr_2O_9$, which also seem to be consistent with spin-1/2 dimers at low temperature, and moreover appear to indicate a gapless quantum spin-liquid ground state [36].

ACKNOWLEDGMENTS

We are grateful to the staff of the Centre for Molecular and Materials Science at TRIUMF for extensive technical support, in particular G. Morris, B. Hitti, D. Arseneau, and I. MacKenzie. We acknowledge useful conversations with S. Johnston and G.E. Granroth and are particularly grateful to S. Streltsov for helping us to understand the intradimer physics of these systems. A portion of this research used resources at the High Flux Isotope Reactor and Spallation Neutron Source, which are U.S. Department of Energy, Office of Science User facilities operated by Oak Ridge National Laboratory. J.Q. acknowledges research funding obtained from NSERC and the FRQNT. R.S. and H.Z. acknowledge the support of Grant No. NSF-DMR-1350002. C.Q. acknowledges the CEM and NSF MRSEC under Grant No. DMR-1420451.

[1] J. G. Cheng, G. Li, L. Balicas, J. S. Zhou, J. B. Goodenough, C. Xu, and H. D. Zhou, Phys. Rev. Lett. **107**, 197204 (2011).

[2] J. A. Quilliam, F. Bert, A. Manseau, C. Darie, C. Guillot-Deudon, C. Payen, C. Baines, A. Amato, and P. Mendels, Phys. Rev. B **93**, 214432 (2016).

[3] B Fak, S. Bieri, E Canévet, L. Messio, C. Payen, M. Viaud, C. Guillot-Deudon, C. Darie, J. Ollivier, and P. Mendels, Phys. Rev. B **95**, 060402 (2017).

[4] T. Dey, A. V. Mahajan, P. Khuntia, M. Baenitz, B. Koteswararao, and F. C. Chou, Phys. Rev. B **86**, 140405 (2012).

[5] H. D. Zhou, E. S. Choi, G. Li, L. Balicas, C. R. Wiebe, Y. Qiu, J. R. D. Copley, and J. S. Gardner, Phys. Rev. Lett. **106**, 147204 (2011).

[6] S. Nakatsuji, K. Kuga, K. Kimura, R. Satake, N. Katayama, E. Nishibori, H. Sawa, R. Ishii, M. Hagiwara, F. Bridges *et al.*, Science **336**, 559 (2012).

[7] J. A. Quilliam, F. Bert, E. Kermarrec, C. Payen, C. Guillot-Deudon, P. Bonville, C. Baines, H. Luetkens, and P. Mendels, Phys. Rev. Lett. **109**, 117203 (2012).

[8] A. Nag, S. Middey, S. Bhowal, S. K. Panda, R. Mathieu, J. C. Orain, F. Bert, P. Mendels, P. G. Freeman, M. Mansson *et al.*, Phys. Rev. Lett. **116**, 097205 (2016).

[9] Y. Shirata, H. Tanaka, A. Matsuo, and K. Kindo, Phys. Rev. Lett. **108**, 057205 (2012).

[10] H. D. Zhou, C. Xu, A. M. Hallas, H. J. Silverstein, C. R. Wiebe, I. Umegaki, J. Q. Yan, T. P. Murphy, J. H. Park, Y. Qiu *et al.*, Phys. Rev. Lett. **109**, 267206 (2012).

[11] T. Susuki, N. Kurita, T. Tanaka, H. Nojiri, A. Matsuo, K. Kindo, and H. Tanaka, Phys. Rev. Lett. **110**, 267201 (2013).

[12] G. Koutroulakis, T. Zhou, Y. Kamiya, J. D. Thompson, H. D. Zhou, C. D. Batista, and S. E. Brown, Phys. Rev. B **91**, 024410 (2015).

[13] G. Quirion, M. Lapointe-Major, M. Poirier, J. A. Quilliam, Z. L. Dun, and H. D. Zhou, Phys. Rev. B **92**, 014414 (2015).

[14] S. V. Streltsov and D. I. Khomskii, Phys. Rev. B **89**, 161112(R) (2014).

[15] S. V. Streltsov and D. I. Khomskii, Proc. Natl. Acad. Sci. USA **113**, 10491 (2016).

[16] S. A. J. Kimber, M. S. Senn, S. Fratini, H. Wu, A. H. Hill, P. Manuel, J. P. Attfield, D. N. Argyriou, and P. F. Henry, Phys. Rev. Lett. **108**, 217205 (2012).

[17] Y. Doi, K. Matsuhira, and Y. Hinatsu, J. Solid State Chem. **165**, 317 (2002).

[18] M. S. Senn, S. A. J. Kimber, A. M. Arevalo Lopez, A. H. Hill, and J. P. Attfield, Phys. Rev. B **87**, 134402 (2013).

[19] J. Rodriguez-Carvajal, Physica B (Amsterdam) **192**, 55 (1993).

[20] The value reported by Senn *et al.* is very far from the values obtained in our work and by Doi *et al.* [17] and, moreover, nearly places the Ru ions outside of the surrounding oxygen octahedra.

[21] K. I. Kugel, D. I. Khomskii, A. O. Sboychakov, and S. V. Streltsov, Phys. Rev. B **91**, 155125 (2015).

[22] L. Seabra and N. Shannon, Phys. Rev. B **83**, 134412 (2011).

[23] R. H. Colman, F. Bert, D. Boldrin, A. D. Hillier, P. Manuel, P. Mendels, and A. S. Wills, Phys. Rev. B **83**, 180416(R) (2011).

[24] A. Yaouanc and P. Dalmas de Réotier, *Muon Spin Rotation, Relaxation, and Resonance: Applications to Condensed Matter* (Oxford University Press, Oxford, 2011).

[25] L. Shlyk, S. Kryukov, V. Durairaj, S. Parkin, G. Cao, and L. E. De Long, J. Magn. Magn. Mater. **319**, 64 (2007).

[26] M. J. P. Gingras, C. V. Stager, N. P. Raju, B. D. Gaulin, and J. E. Greedan, Phys. Rev. Lett. **78**, 947 (1997).

[27] P. Schiffer, A. P. Ramirez, D. A. Huse, P. L. Gammel, U. Yaron, D. J. Bishop, and A. J. Valentino, Phys. Rev. Lett. **74**, 2379 (1995).

[28] J. A. Quilliam, S. Meng, H. A. Craig, L. R. Corruccini, G. Balakrishnan, O. A. Petrenko, A. Gomez, S. W. Kycia, M. J. P. Gingras, and J. B. Kycia, Phys. Rev. B **87**, 174421 (2013).

[29] W. G. Bisson and A. S. Wills, J. Phys. Condens. Matter **20**, 452204 (2008).

[30] C. C. Paulsen, S. J. Williamson, and H. Maletta, Phys. Rev. Lett. **59**, 128 (1987).

[31] L. P. Le, A. Keren, G. M. Luke, B. J. Sternlieb, W. D. Wu, Y. J. Uemura, J. H. Brewer, T. M. Riseman, R. V. Upusani, L. Y. Chiang *et al.*, Phys. Rev. B **48**, 7284 (1993).

[32] S. J. Blundell and F. L. Pratt, J. Phys. Condens. Matter **16**, R771 (2004).

[33] N. Katayama, K. Kimura, Y. Han, J. Nasu, N. Drichko, Y. Nakanishi, M. Halim, Y. Ishiguro, R. Satake, E. Nishibori *et al.*, Proc. Natl. Acad. Sci. USA **112**, 9305 (2015).

[34] Y. Ishiguro, K. Kimura, S. Nakatsuji, S. Tsutsui, A. Q. R. Baron, T. Kimura, and Y. Wakabayashi, Nat. Commun. **4**, 1 (2013).

[35] K. Sugii, M. Shimozawa, D. Watanabe, Y. Suzuki, M. Halim, M. Kimata, Y. Matsumoto, S. Nakatsuji, and M. Yamashita, Phys. Rev. Lett. **118**, 145902 (2017).

[36] T. Dey, M. Majumder, J. C. Orain, A. Senyshyn, M. Prinz-Zwick, F. Bert, P. Khuntia, N. Büttgen, A. A. Tsirlin, and P. Gegenwart, arXiv:1702.08305.